Mineralogy and Petrology (2004) 81: 219–234
DOI 10.1007/s00710-004-0040-x

Mineralogy and Petrology

OH defects in cassiterite

Z. Losos[1] and **A. Beran**[2]

[1] Institute of Geological Sciences, Masaryk University Brno, Czech Republic
[2] Institut für Mineralogie und Kristallographie, Universität Wien-Geozentrum, Austria

Received October 15, 2003; accepted February 4, 2004
Editorial handling: E. Libowitzky

Summary

Two infrared (IR) spectral types are discerned in cassiterites with OH defect concentrations ranging from several wt. ppm H_2O in synthetic melt-grown samples up to 0.017 wt.% in natural samples of hydrothermal origin. Spectrum type I is characterised by one sharp band centred at 3255 cm^{-1}, type II spectra reveal an additional band group centred around 3340 cm^{-1}, which is clearly correlated with the presence of Ti. Both OH band groups are strongly polarised with maximum absorption perpendicular to the c-axis. Type I spectra prevail in nearly colourless samples, type II spectra typically occur in light to dark brown cassiterites, bearing essentially higher amounts of minor elements, especially Ti, Nb, Ta, W, Zr, and Fe. The total amount of water is not significantly correlated with the minor element content. It is concluded that different OH concentrations reflect different water activities prevalent during the formation of cassiterite crystals in different geological environments.

Introduction

The presence of OH defects in nominally anhydrous minerals (NAMS) can strongly influence their physical and chemical properties (e.g. *Rossman*, 1990). The OH concentration may vary as a function of the geological environment (*Ingrin* and *Skogby*, 2000). It is suggested that also crystal chemical or compositional factors control the incorporation of OH groups (*Andrut* et al., 2003). The recognition of OH defects in natural cassiterite was initially based on measurements of the electrical conductivity by *Kohnke* (1962). *Beran* and *Zemann* (1971) and *Katiyar* et al. (1971) established the presence of OH groups in cassiterites from natural occurrences by polarised infrared (IR) spectroscopy. OH groups in cassiterite were also reported by *Rhein* (1972) on the basis of electron paramagnetic

resonance (EPR) measurements. Extended EPR studies revealed the presence of four paramagnetic centres, one of them, the I centre, is connected with the substitution process $Sn^{4+} + O^{2-} = Fe^{3+} + OH^{-}$, (*Dusausoy* et al., 1988; *Ruck* et al., 1989). This substitution mechanism was also proposed by *Möller* et al. (1988) on the basis of Mössbauer spectroscopic results on the oxidation state of Fe.

Infrared (IR) spectroscopy provides an extremely sensitive method for detecting trace hydrogen bonded to oxygen in the structure of various NAMS (*Beran* and *Libowitzky*, 2003). The structural information is evaluated from the energy of the OH stretching vibrations, as these depend on the hydrogen bond lengths and strengths and consequently on the cations to which the OH groups are coordinated. Additional information is obtained by using polarised IR radiation. The pleochroic scheme allows to impose defined constraints on the orientation of the OH dipoles. The intensity of IR absorption bands provides information on the OH defect concentration.

Cassiterites from different localities show different absorption patterns. A doublet band with maxima around 3250 and 3350 cm^{-1} was reported by *Beran* and *Zemann* (1971) in cassiterite crystals cut parallel to the c-axis from Cinovec, Czech Republic and Araca, Bolivia. *Katiyar* et al. (1971) presented a polarised IR spectrum measured at 100 K with significant bands at 3223, 3264, 3279, 3338 and 3358 cm^{-1}. Polarised single-crystal spectra of a sample from Vietnam were presented by *Bréhat* et al. (1990) showing bands at 3170, 3260 and 3345 cm^{-1}. Cassiterites from Cinovec, Czech Republic and Cornwall, England studied by *Maldener* et al. (2001) are characterised by bands centred around 3250 and 3350 cm^{-1}. The OH absorption bands of all cassiterite samples are strongly pleochroic. Maximum absorption occurs when the electric vector of the polarised radiation vibrates perpendicular to the c-axis, thus indicating OH groups at the oxygen site of the tetragonal rutile-type structure, oriented approximately perpendicular to the plane of the three coordinating Sn atoms (*Beran* and *Zemann*, 1971; *Katiyar* et al., 1971).

The aim of this paper is to establish the presence and quantity of OH defects in cassiterites from different localities by FTIR microspectroscopy and to characterise their structural incorporation mechanisms related to chemical composition and geological provenance.

Experimental

Samples

Cassiterite single-crystals of gem-quality were isolated, and oriented plates cut and polished parallel to the c-axis were prepared. Only samples of excellent optical quality that proved to be free of microscopic inclusions and impurities were used for the measurements. The accurate thicknesses of the investigated crystal slabs, ranging around 0.05 cm are given in Table 1. Cassiterite samples originate from localities in the Czech Republic, Portugal, France, England, Russia, Mongolia, Bolivia and Brazil, representing also different geological environments and genetic types. Additionally, two synthetic cassiterite crystals grown on native Sn were studied. The sample characteristics are summarised in Table 1.

Table 1. *Localities, genetic type, thickness and colour of the crystal slabs. H_2O contents were calculated on basis of Beer's law using the integral molar absorption coefficient $\varepsilon_i = 65\ 000\, l \cdot mol^{-1}\ H_2O \cdot cm^{-2}$ (*Maldener *et al., 2001)*

Sample no.	Locality	Genetic type	Thickness (in cm)	Colour[1]	H_2O content (in wt.%)
4	Krupka, Czech Republic	Greisen	0.045	light brown	0.0049
6	Cínovec, Czech Republic	Greisen	0.049	light brown	0.0110
10	Modoto, Mongolia	Greisen	0.049	light brown	0.0093
11	Panasqueira, Portugal	Hydrothermal vein deposit	0.053	dark brown	0.0120
12	La Villedas, France	?	0.052	colourless	0.0032
13	Potosi, Bolivia	Cassiterite-sulphide type deposit	0.053	yellow	0.0170
14	Synthetic cassiterite	Tin melt	0.053	colourless	0.0002
15	Synthetic cassiterite	Tin melt	0.054	yellow	0.0008
16	Horní Slavkov, Czech Republic	Greisen/ quartz vein	0.053	reddish brown	0.0090
17	Bahia, Brazil	? cut gemstone	0.111	yellow	0.0032
18	Russia	?	0.061	light brown	0.0082

[1] Observed under the microscope in regions used for the FTIR spectroscopic water determination

Under the microscope, some samples show a distinct colour zoning, ranging from colourless to dark-brown. The observed growth textures comprise concentric banding, oscillatory zoning and sector zoning, sometimes occurring in dimensions within few tenths of a millimeter.

IR spectroscopy

Polarised single-crystal spectra were recorded from 4000–2700 cm^{-1} with a Perkin-Elmer FTIR spectrometer 1760X combined with a Perkin-Elmer FTIR microscope using 0.60 numerical aperture Cassegrain objectives and a liquid nitrogen-cooled MCT detector. Background and sample spectra were obtained from 64 scans each in air and in the sample crystal with 4 cm^{-1} resolution. A gold wire grid polariser was used with an extinction ratio better than 1:100. Measuring fields were chosen according to the dimensions of microscopically homogeneous parts of the crystals with clearly defined extinction directions; considering a sufficient quality of the spectra, the minimum size was restricted to about $50 \times 50\,\mu m$. After background correction the spectra were deconvoluted in the 3400–3200 cm^{-1} range into Voigt-shaped absorption bands, and their band centre, full width at half maximum and integrated absorbance were determined with the program PeakFit (Jandel Scientific).

Chemical analyses of selected cassiterite slabs were performed with an automated ARL-SEMQ electron microprobe at 15 kV operating voltage and 15 nA

sample current measured on benitoite. The analyses were corrected by the modified correction procedures of *Armstrong* (1984) and *Love* and *Scott* (1978). Trace element concentrations for two samples were provided by inductively coupled plasma mass spectrometry (ICP-MS) using a Perkin-Elmer Elan 6100 instrument. The samples were partially disintegrated with NaOH at 700 °C in a Ni crucible and diluted in H_2O.

Quantitative water determination

In anisotropic crystals normally the sum of the integral absorbances A_i measured with polarised radiation in principal axis directions of oriented crystal sections result in accurate values of the OH defect concentration (*Libowitzky* and *Rossman*, 1996; *Beran* and *Libowitzky*, 2003). As expressed by Beer's law the integral absorption coefficient α_i (cm^{-2}) = A_i (cm^{-1})/t (sample thickness in cm) is directly related by the integral molar absorption coefficient ε_i ($l \cdot mol^{-1} H_2O \cdot cm^{-2}$) to the concentration c ($mol \cdot l^{-1}$). The water content in wt.% is calculated using the relationship $c_{H_2O} = (1.8/D) \cdot (\alpha_i/\varepsilon_i)$, where D is the density of the mineral in ($g \cdot cm^{-3}$) (*Beran* et al., 1993). The integral molar OH absorption coefficient was determined for cassiterite on the basis of nuclear reaction analysis by *Maldener* et al. (2001) and amounts to $\varepsilon_i = 65\ 000 l \cdot mol^{-1} H_2O \cdot cm^{-2}$. As discussed by *Maldener* et al. (2001) this value is significantly smaller than that expected from the linear calibration curves given by *Paterson* (1982) and *Libowitzky* and *Rossman* (1997) and is probably more realistic for the present form of OH defects.

Results

Representative polarised OH absorption spectra of selected cassiterite samples with the electric vector of the IR radiation vibrating perpendicular to the c-axis are summarised in Figs. 1, 2 and 3. Two main spectral types can be discerned. Type I is represented by synthetic cassiterite samples consisting of a single narrow band centred around 3255 cm^{-1} and a weak shoulder around 3280 cm^{-1} (Fig. 1a). These samples are colourless to light-brown and contain only trace amounts of Ta, Nb, W, Zr and Fe. In natural samples included in type I and represented in Fig. 1b by the Bahia cassiterite (no. 17), the 3255 cm^{-1} band is split into two bands with an additional maximum at 3265 cm^{-1}. Also this sample contains only very minor amounts of Ta, Nb and Zr. The band positions of selected samples are summarised in Table 2. The average values of minor elements microprobe analyses performed in crystal parts also analysed by FTIR microspectroscopy are given in Table 3. Type II spectra are characterised by the presence of the type I spectral group plus an additional band group at higher energies, centred around 3340 cm^{-1}. Band splitting within this high-energy group can be observed by the presence of additional bands centred around 3325, 3350 and 3365 cm^{-1}. Usually the band intensities of the high-energy band group are lower than those of the low-energy band group (see Fig. 2a, cassiterite no. 10), but as documented by the brown to dark-brown Panasqueira cassiterite (no. 11), examples also exist for type II spectra with high intensities of the high-energy band group (Fig. 2b). It is obvious that in coloured samples the content of the minor elements Ti, Ta, Nb, W and Fe is slightly

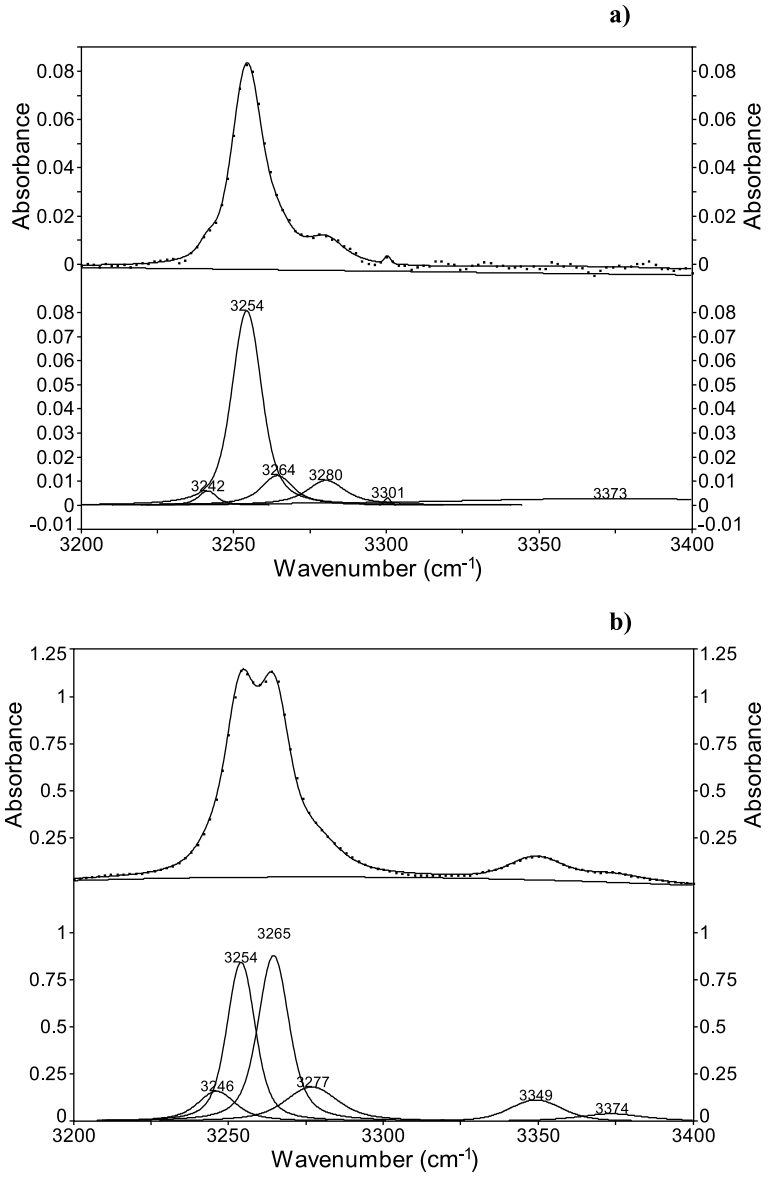

Fig. 1. Polarised single-crystal spectra in the OH stretching vibrational range, with the electric vector of the polarised radiation vibrating perpendicular to the c-axis. The lower part of the figures shows the results of the band deconvolution procedure. **a** Synthetic cassiterite no. 14, representing type I spectrum. **b** Cassiterite from Bahia no. 17, natural sample representing type I spectrum. Note the different absorbance scales due to the great difference in the OH defect concentration

enhanced. The mostly dominating Ti content is clearly related to the presence of the band at 3340 cm^{-1}. In dark-coloured samples the background of the OH absorption bands is significantly enhanced.

Trace element analyses performed on the Krupka (no. 4) and Modoto sample (no. 10) by ICP-MS revealed, in addition to the elements determined by microprobe measurements, significant amounts of Mg, Al and Mn. The two crystals which were

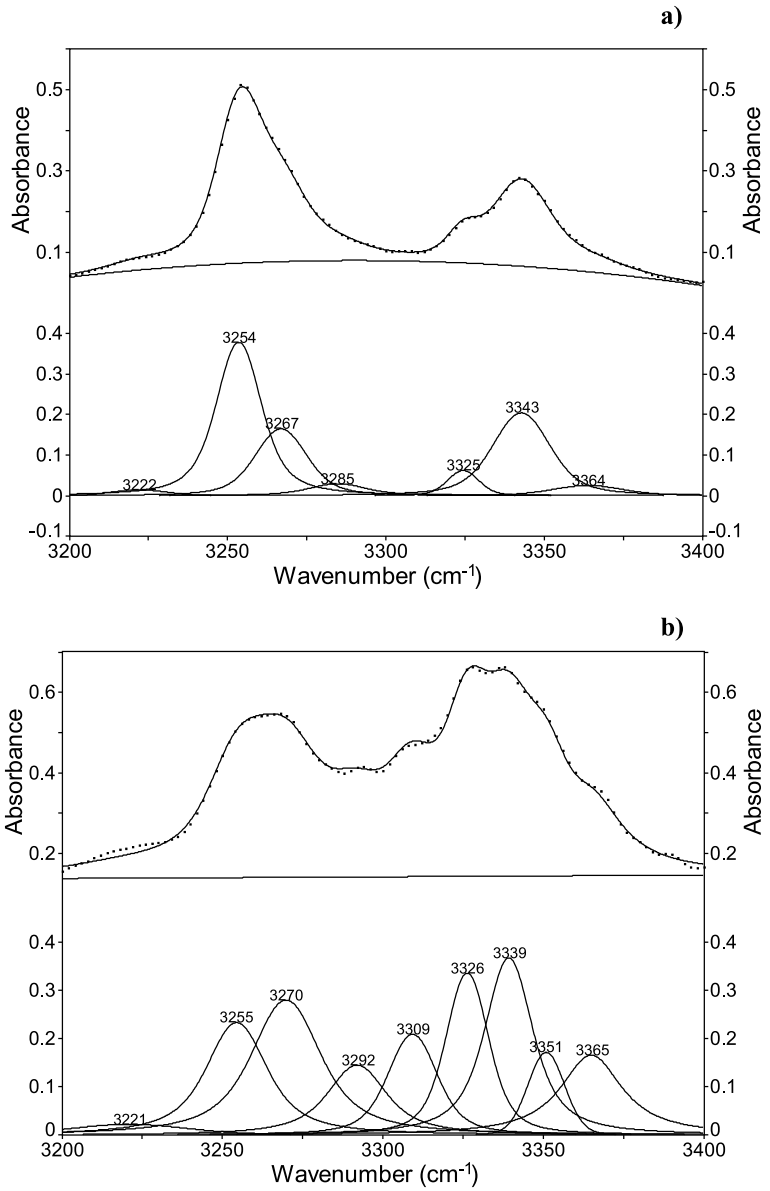

Fig. 2. Polarised single-crystal spectra in the OH stretching vibrational range, with the electric vector of the polarised radiation vibrating perpendicular to the c-axis. The lower part of the figures shows the results of the band deconvolution procedure. **a** Cassiterite from Modoto no. 10, representing type II spectrum. **b** Cassiterite from Panasqueira no. 11, representing type II spectrum with a dominating high-energy band group

Fig. 3. Polarised single-crystal spectra in the OH stretching vibrational range of the Russian cassiterite no. 18 showing a distinct colour zoning, with the electric vector of the polarised radiation vibrating perpendicular to the c-axis. The lower part of the figures shows the results of the band deconvolution procedure. **a** Colourless, **b** dark brown, **c** black crystal part

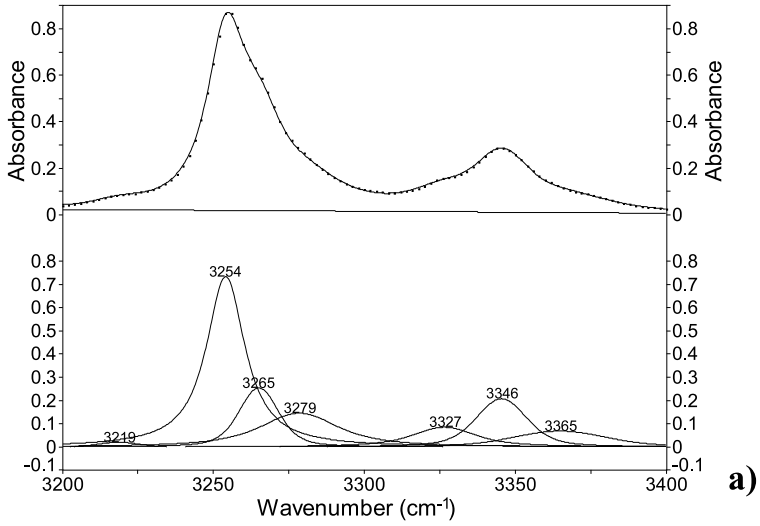
Absorbance
Wavenumber (cm-1)
3254
3265
3279
3219
3327
3346
3365

a)

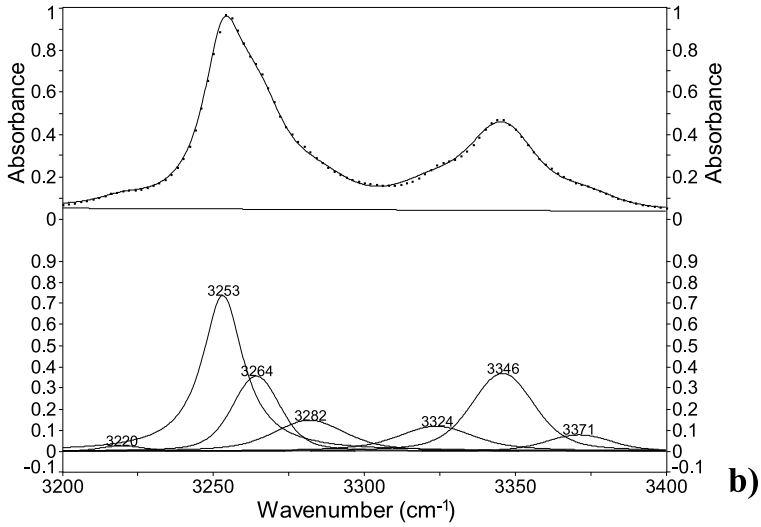
Absorbance
Wavenumber (cm-1)
3253
3264
3282
3220
3324
3346
3371

b)

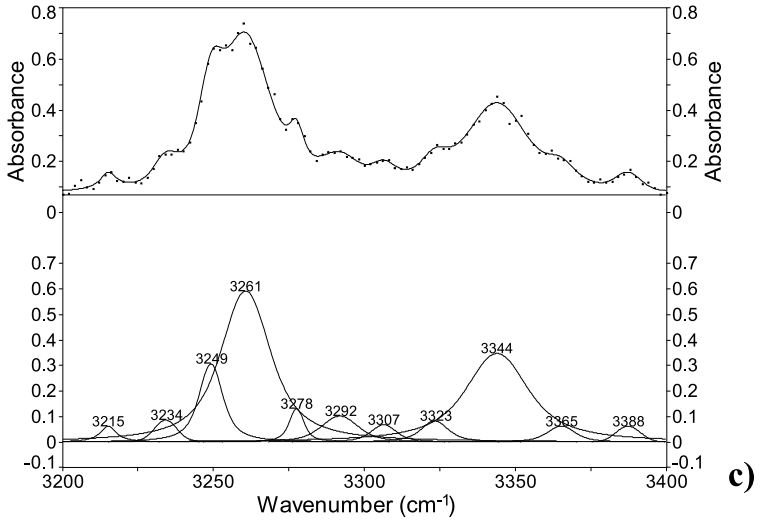
Absorbance
Wavenumber (cm-1)
3261
3249
3278
3292
3307
3215
3234
3323
3344
3365
3388

c)

Table 2. *OH band positions in cm^{-1} of cassiterites from different localities. Wavenumber values with deviations of $\pm 4\ cm^{-1}$ are listed within one horizontal line. The values refer to the absorption bands used for the determination of the water content. For localities see Table 1. For the Russian cassiterite sample no. 18, the polarised spectra were measured on (001) slabs showing a distinct colour zoning. For the calculation of the water content on basis of Beer's law ($\varepsilon_i = 65\ 000\ l \cdot mol^{-1} H_2O \cdot cm^{-2}$) the weak component parallel to the c-axis was derived from the average pleochroic ratio of 1/10, determined for the samples cut parallel to the c-axis. Relative band intensity scale:* vs *very strong,* s *strong,* m *moderate,* w *weak,* vw *very weak*

Sample no.	4	6	10	11	12	13	14	15	16	17
			3222/vw	3221/vw	3219/w			3224/vw		
							3242vw			3246/w
	3254/vs	3254/vs	3254/vs	3255/vs	3255/vs	3254/vs	3254/vs	3255/vs	3255/vs	3254/vs
	3265/s	3265/s	3267/s	3270/vs	3268/s	3267/s	3264/w		3268/m	3265/vs
	3277/m	3279/m	3285/vw		3280/m	3280/m	3280/w	3282/w	3278/w	3277/m
				3292/m						
				3309/s						
	3325/w	3325/w	3325/m	3326/vs	3327/m				3326/m	
									3334/w	
	3342/s	3342/s	3343/vs	3339/vs	3341/s				3345/s	
		3350/m		3351/m	3353/w	3347/m				3349/m
	3358/vw								3357/w	
			3364/vw	3365/m	3367/vw	3364/w			3369/w	
		3372/w				3375/m				3374/vw
						3391/w			3391/w	

(*continued*)

Table 2 (*continued*)

Sample no./measured area	18/6	18/2	18/1	18/5	18/3	18/4
Colour of analysed area	colourless	light brown	light brown	pinkish brown	dark brown	black
	3219/vw	3219/vw	3217/vw	3219/vw	3220/vw	3215/vw
						3234/w
	3254/vs	3254/vs	3253/vs	3254/vs	3253/vs	3249/m
	3265/s	3265/m	3264/s	3266/s	3264/s	3261/vs
	3279/w	3277/m	3279/m	3282/w	3282/w	3278/m
						3292/w
						3307/w
	3327/w	3325/m	3325/w	3329/w	3324/vw	3328/w
	3346/s	3345/s	3345/s	3346/s	3346/vs	3344/vs
			3360/w		3371/w	
	3365/w	3367/w		3367/w		3365/w
						3388/w
H_2O content (in wt.%)	0.0059	0.0082	0.0090	0.0076	0.0083	0.0083

Table 3. *Minor elements microprobe analyses of the cassiterite samples. Average values of three point analyses in wt.%, standard deviations in parentheses. Values of single point analyses from profile measurements are given for samples no. 13 and 18, representing cassiterites with distinct colour zoning (Analyst:* F. Brandstätter, *Naturhistorisches Museum, Wien).* n.d. *not detected*

Sample no.	TiO_2	ZrO_2	FeO	Ta_2O_5	Nb_2O_5	WO_3
4	0.23 (5)	0.04 (1)	<0.02	0.06 (5)	0.04 (4)	0.09 (8)
6	0.17 (4)	0.02 (2)	0.07 (2)	0.10 (8)	0.03 (2)	0.09 (9)
10	0.24 (3)	n.d.	<0.02	0.06 (4)	n.d.	<0.02
11	0.50 (2)	0.02 (2)	0.02 (1)	0.08 (8)	<0.02	0.05 (5)
12	0.17 (2)	0.02 (2)	0.02 (1)	n.d.	<0.02	0.04 (4)
14	n.d.	0.03 (2)	<0.02	0.05 (3)	<0.02	0.02 (2)
15	n.d.	n.d.	0.06 (3)	0.10 (9)	n.d.	n.d.
16	0.30 (7)	0.02 (2)	0.05 (4)	<0.02	0.02 (2)	0.32 (9)
17	n.d.	0.02 (2)	n.d.	0.05 (5)	<0.02	n.d.
13/1	n.d.	0.05	0.40	0.10	n.d.	0.14
13/2	n.d.	n.d.	0.33	n.d.	n.d.	0.69
13/3	<0.02	n.d.	0.30	0.10	n.d.	0.69
13/4	n.d.	n.d.	0.36	n.d.	n.d.	0.36
13/5	n.d.	n.d.	0.34	n.d.	n.d.	n.d.
13/6	n.d.	n.d.	0.30	0.03	n.d.	n.d.
13/7	n.d.	0.05	0.17	n.d.	n.d.	n.d.
13/8	n.d.	n.d.	0.14	0.03	n.d.	n.d.
13/9	0.02	n.d.	0.09	0.03	n.d.	n.d.
13/10	n.d.	n.d.	0.09	n.d.	0.03	0.40
18/1	0.13	0.05	0.07	0.03	0.03	n.d.
18/2	0.09	n.d.	0.06	n.d.	0.03	n.d.
18/3	0.14	n.d.	0.03	n.d.	0.03	n.d.
18/4	0.10	n.d.	0.03	0.14	n.d.	n.d.
18/5	0.14	0.05	0.06	0.21	0.03	0.04
18/6	0.09	n.d.	n.d.	0.17	0.03	0.11
18/7	0.10	n.d.	n.d.	0.07	0.03	0.07

available for the trace element analyses showed differently coloured parts. After breaking to small pieces, both crystals were divided in a light and dark brown species and separately analysed. The values are summarised in Table 4. Very minor amounts of Ca, Si and P were detected by the X-ray fluorescence method. As indicated by the Y value, rare earth elements are generally below 1 wt. ppm. It is worth to note the relatively high amounts of Hf, especially in comparison with the relatively low Zr values, indicating a highly fractionated fluid phase. The IR spectra of differently coloured zones of a large crystal from the Russian locality (no. 18) clearly demonstrate the varying intensity ratios of the high- and low-energy band groups related to the colour of the crystal (Fig. 3a–c). As evident from Table 2, except the colourless crystal part which shows a slightly lower water content, the OH defect concentration within differently coloured zones remains nearly constant, i.e. the total amount of water is not significantly correlated with the total amount of minor elements.

Table 4. *Trace element content determined by ICP-MS for the cassiterite samples no. 4 and 10 in wt. ppm. Light and dark parts of the crystals were separately analysed. Errors are in the range around 10 rel.% (Analyst:* P. Spindler, *ARC Seibersdorf Research)*

Elements	Sample no. 4		Sample no. 10	
	light	dark	light	dark
Li	7	3	2	2
Be	<1	<1	<1	<1
Mg	160	140	120	170
Al	210	170	270	290
Ti	2600	3200	3900	4100
Mn	100	250	60	81
Fe	630	490	650	700
Rb	<10	<10	<10	<10
Y	<1	<1	<1	<1
Zr	120	150	170	200
Nb	230	240	230	300
Sb	5	5	5	4
Cs	7	7	7	6
Hf	10	13	91	110
Ta	22	16	100	85
W	260	230	84	140
Tl	<0.1	<0.1	<0.1	<0.1
Pb	8	4	13	15
Bi	<1	<1	<1	<1
Th	<0.1	<0.1	<0.1	<0.1
U	5	12	6	11

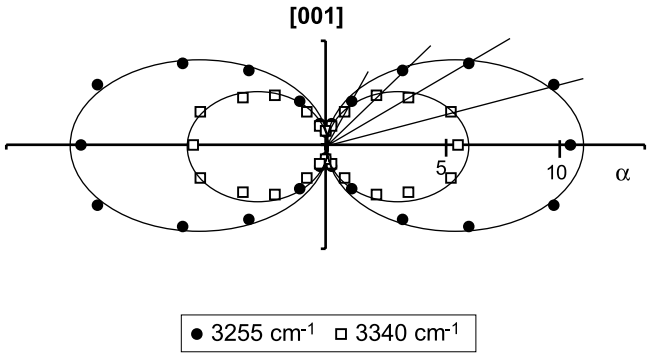

Fig. 4. Linear absorption coefficient of the OH bands at 3255 cm^{-1} (symbol circles) and 3340 cm^{-1} (symbol squares) correlated to the rotation of the vector of the polarised radiation on a cassiterite plate polished parallel to the c-axis (cassiterite from Modoto no. 10)

Both band groups are strongly pleochroic with maximum absorption perpendicular to the c-axis (Fig. 4). However, it must be noted that slight differences in the pleochroic ratio do exist, thus indicating slightly different deviations of the OH

dipole directions from the normal to the c-axis. As an average, the minimum/maximum ratio amounts to 1/10. The IR spectroscopically determined absolute water content is extremely low for the synthetic samples and amounts to values below 10 wt. ppm (Table 1). The water content of the natural samples ranges up to 0.017 wt.%. This value is represented by a samples from hydrothermal vein deposit (Potosi no. 13). The Panasqueira sample, containing 0.012 wt.% H_2O, is also of hydrothermal origin. Cassiterites from greisen occurrences typically contain 0.009 wt.% H_2O (Table 1).

Discussion

Type I spectrum with the characteristic band at 3255 cm^{-1} is the typical absorption pattern of synthetic cassiterite and colourless to very light-brown natural samples which represent the purest phases (e.g. Bahia no. 17). Accordingly, the band at 3255 cm^{-1} is assigned to OH defects of the ''ideal'' structure where the OH defect sites are coordinated to three Sn atoms. The second group of bands centred around 3340 cm^{-1}, which is the characteristic feature of type II spectra is mostly prominent in brown to dark-brown coloured samples containing relatively high amounts of minor elements. Ti is clearly correlated with the intensity of the 3340 cm^{-1} band. This is demonstrated in Fig. 5 showing the correlation between the ratio of the linear absorbances of the 3340 and 3255 cm^{-1} bands and the TiO_2 content. Consequently the 3340 cm^{-1} band is assigned to OH defects where Ti is part of the coordinating cations. This band could be due to OH defects, coordinated by two Sn and one Ti atom. However, charge balance must be provided by the presence of di- or trivalent cations; we also have to consider the presence of Ti^{3+}, or vacant cation sites neighbouring the OH defects.

From the band position information on the hydrogen bond system can be obtained. Empirical correlation diagrams of OH stretching frequencies versus O–H. . .O distances were presented by *Novak* (1974) and especially for minerals by *Libowitzky* (1999). From these diagrams a relatively strong hydrogen bond with

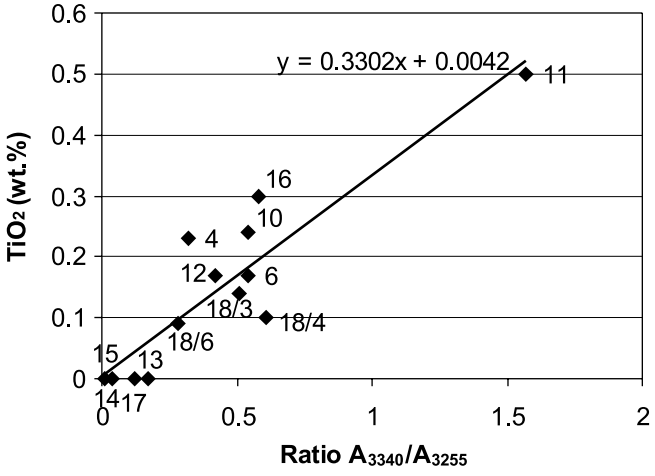

Fig. 5. Ratio of the linear absorbances of the 3340 and 3255 cm^{-1} bands plotted versus the analytical TiO_2 content in wt.%, demonstrating a significant correlation. Sample no. refer to Table 1

O–H. . .O distances of about 2.75–2.80 Å can be deduced. Assuming an OH dipole direction approximately perpendicular to the plane of the three coordinating cations, a strong local distortion of the structure would be required. However, hydrogen bond distances can only be predicted with limited precision from these correlation diagrams, especially for OH defect structures.

The band splitting within the low-energy band group centred at 3255 cm^{-1} with additional bands at 3265 and 3280 cm^{-1} can be explained by a different coordination of the acceptor oxygen atoms of the hydrogen bonds. In the ideal case of the SnO_2 structure also the acceptor oxygen is coordinated by three Sn atoms. The replacement of Sn, coordinating the acceptor oxygen, by one of the minor elements would result in a slight shift of the band maximum to slightly higher wavenumbers. This assignment is supported by the fact that the intensities of these two additional bands are correlated to the intensity of the high-energy band group, that is clearly demonstrated in the spectrum of the Panasqueira cassiterite (Fig. 2b, no. 11). The same situation holds for the split bands of the high-energy band group, where both, the donor and the acceptor oxygen of the O–H. . .O bond have a complex coordination with different cations present as minor elements (Tables 3 and 4). Additional absorption bands can also be explained by the presence of cation vacancies which would result in a two-fold coordination of the OH defect positions.

Geochemical aspects

Many papers are dealing with the geochemistry of cassiterites with respect to the frequently observed colour zoning. According to *Farmer* et al. (1991) cathodoluminescence of zoned cassiterites is controlled by the substitution of Ti, Fe and W for Sn in the crystal structure. Ti and W behave as luminescence activators whereas Fe quenches luminescence. Based on scanning electron microscopy, electron microprobe and Mössbauer spectroscopy, *Möller* et al. (1988) concluded that the substitution of Sn by (Ta, Nb) + Fe^{2+} and by W + Fe^{3+} are important mechanisms for the structural incorporation of these elements in cassiterite and that this incorporation is indistinguishable from the presence of submicroscopic inclusions of (Ta, Nb) oxide minerals of corresponding composition. A detailed microprobe study of cassiterites from tin and tungsten deposits of Portugal was presented by *Neiva* (1996), showing that the darker zones of the cassiterite samples have essentially more Nb, Ta and Fe than the lighter zones which are nearly pure SnO_2. The dark zones show exsolved columbite-tantalite and ixiolite, rarely tapiolite, rutile and ilmenite. Microprobe analyses of dark-brown pegmatitic cassiterites from the Czech locality Recice (*Novak*, 1999) reveal Ta_2O_5 contents up to 2.2 wt.% and FeO contents up to 0.6 wt.%; the Nb_2O_5 contents average around 1 wt.%. Cassiterites from tin and tungsten deposits of Spain have been studied by microprobe and EPR spectroscopy by *Izoret* et al. (1985). The dark zones are enriched in Ti, Fe, Nb and Ta, in the light coloured zones only Ti was detected in very small amounts. An EPR study of *Ruck* et al. (1989) confirmed the relatively high concentrations of Nb and Fe in dark-coloured parts of cassiterites in comparison to the Nb and Fe poor and clearer crystal parts.

These studies on the chemical variability of cassiterites agree with the observations of the present study (see Tables 3 and 4). The spectral types are related to the

colour of the cassiterite crystals. However, a significant correlation with the spectral type can only be established for the Ti content. No bands are especially correlated to the presence of Ta, Nb or W. No indications exist for the expected correlation of the OH concentration or of a spectral feature with the Fe content. This observation slightly supports the idea that part of these elements are present in form of submicroscopic phases, thus not available for charge compensation mechanisms. The detailed FTIR microspectroscopic study of the zoned Russian crystal (see Fig. 3) showed that the OH concentration remains practically constant within the crystal, independent from their colour and spectral type, and that association of the OH incorporation with the minor element content is limited.

Due to the different water contents of the individual samples it is evident that there is an environmental factor, distinct from crystal chemistry and charge balance effects. It is concluded that OH incorporation is only partly related to the substitution of tri- and penta-valent cations for Sn, but also gives an indication for different water activities prevalent during the formation of cassiterite crystals in the corresponding geological environment. This behaviour is similar to that observed for OH defects in rutiles from geologically different occurrences (*Hammer* and *Beran*, 1991; *Vlassopoulos* et al., 1993). Compared to rutile, showing water contents up to tenths wt.%, the OH concentrations in cassiterite appear to be generally lower.

The "varlamoffite problem"

In a Russian paper by *Sidorenko* et al. (1993) the secondary tin mineral varlamoffite was redefined (for English abstract see *Jambor* et al., 1995). Varlamoffite has a cassiterite-like structure with the generalised formula $Sn_{1-x}Fe_xO_{2-x}(OH)_x$. The studied sample from the Tigrinoe deposit has the average composition $Sn_2FeO_5(OH)$. The IR spectrum in the OH stretching vibrational region is characterised by a broad absorption band centred around 3400 cm^{-1}. A weaker, but also broad band is located around 3200 cm^{-1}. The IR spectrum of varlamoffite from the Australian Sardine mine published by *Taylor* et al. (1970) shows a broad band around 3300 cm^{-1}. No similarities are evident between the OH absorption features of cassiterite and varlamoffite. Based on these spectroscopic data and as originally discussed by *Beran* and *Zemann* (1971), the presence of varlamoffite as an included secondary hydrous phase can be ruled out. Further it is concluded that the observed hydrogen content of the cassiterite crystals presents a primary trace element incorporation and not the result of late hydrothermal alteration processes.

Acknowledgements

Thanks are due to *F. Brandstätter*, Naturhistorisches Museum, Wien, for assistance with the microprobe, to *M. A. Götzinger* for the completion of SE images and to *P. Spindler*, ARC Seibersdorf Research for the ICP-MS analyses. We thank *A. Wagner* for sample preparation. The remarks and suggestions of two anonymous reviewers have essentially improved the clarity of the paper. This work was supported by the European Commission through the Programme "Human Potential – Research Training Networks", No. RTN1-1999-00353.

References

Andrut M, Brandstätter F, Beran A (2003) Trace hydrogen zoning in diopside. Mineral Petrol 78: 231–241

Armstrong JT (1984) Quantitative analysis of silicate and oxide minerals: a reevaluation of ZAF corrections and proposal for new Bence-Albee coefficients. In: *Romig AD Jr, Goldstein JI* (eds) Microbeam analysis. San Francisco Press, San Francisco, pp 208–212

Beran A, Zemann J (1971) Messung des Ultrarot-Pleochroismus von Mineralen. XI. Der Pleochroismus der OH-Streckfrequenz in Rutil, Anatas, Brookit und Cassiterit. Tschermaks Mineral Petrogr Mitt 15: 71–80

Beran A, Libowitzky E (2003) IR spectroscopic characterization of OH defects in mineral phases. Phase Trans 76: 1–15

Beran A, Langer K, Andrut M (1993) Single crystal infrared spectra in the range of OH fundamentals of paragenetic garnet, omphacite and kyanite in an eclogitic mantle xenolith. Mineral Petrol 48: 257–268

Bréhat F, Wyncke B, Léonard JM, Dusausoy Y (1990) Infrared reflectivity spectra of single crystal cassiterites. Phys Chem Minerals 17: 191–196

Dusausoy Y, Ruck R, Gaite JM (1988) Study of the symmetry of Fe^{3+} sites in SnO_2 by electron paramagnetic resonance. Phys Chem Minerals 15: 300–303

Farmer CB, Searl A, Halls C (1991) Cathodoluminescence and growth of cassiterite in the composite lodes at South Crofty Mine, Cornwall, England. Mineral Mag 55: 447–458

Hammer VMF, Beran A (1991) Variations in the OH concentration of rutiles from different geological environments. Mineral Petrol 45: 1–9

Ingrin J, Skogby H (2000) Hydrogen in nominally anhydrous upper-mantle minerals: concentration levels and implications. Eur J Mineral 12: 543–570

Izoret L, Marnier G, Dusausoy Y (1985) Caractérisation cristallochimique de la cassitérite des gisements d'étain et de tungstène de Galice, Espagne. Can Mineral 23: 221–231

Jambor JL, Pertsev NN, Roberts AC (1995) New mineral names: Varlamoffite. Am Mineral 80: 850

Katiyar RS, Dawson P, Hargreave MM, Wilkinson GR (1971) Dynamics of the rutile structure III. Lattice dynamics, infrared and Raman spectra of SnO_2. J Phys C: Solid St Phys 4: 2421–2431

Kohnke EE (1962) Electrical and optical properties of natural stannic oxide crystals. J Phys Chem Solids 23: 1557–1562

Libowitzky E (1999) Correlation of O–H stretching frequencies and O–H. . .O hydrogen bond lengths in minerals. Mh Chem 130: 1047–1059

Libowitzky E, Rossman GR (1996) Principles of quantitative absorbance measurements in anisotropic crystals. Phys Chem Minerals 23: 319–327

Libowitzky E, Rossman GR (1997) An IR absorption calibration for water in minerals. Am Mineral 82: 1111–1115

Love G, Scott VD (1978) Evaluation of a new correction procedure for quantitative electron microprobe analysis. J Phys D18: 1233

Maldener J, Rauch F, Gavranic M, Beran A (2001) OH absorption coefficients of rutile and cassiterite deduced from nuclear reaction analysis and FTIR spectroscopy. Mineral Petrol 71: 21–29

Möller P, Dulski P, Szacki W, Malow G, Riedel E (1988) Substitution of tin in cassiterite by tantalum, niobium, tungsten, iron and manganese. Geochim Cosmochim Acta 52: 1497–1503

Neiva AMR (1996) Geochemistry of cassiterite and its inclusions and exsolution products from tin and tungsten deposits in Portugal. Can Mineral 34: 745–768

Novak A (1974) Hydrogen bonding in solids. Correlation of spectroscopic and crystallographic data. Structure Bonding 18: 177–216

Novak M (1999) Cassiterite and tusionite as monitors of B and Sn behaviour in the elbaite pegmatite at Recice near Nové Mesto na Morave, western Moravia, Czech Republic. N Jb Miner Mh 1999: 481–493

Paterson MS (1982) The determination of hydroxyl by infrared absorption in quartz, silicate glasses and similar materials. Bull Mineral 105: 20–29

Rhein W (1972) Elektronen-Spin-Resonanz und ENDOR-Messungen an Fe^{3+} und Cr^{3+} in Zinndioxid. Z Naturforsch 27a: 741–749

Rossman GR (1990) Hydrogen in ''anhydrous'' minerals. Nucl Instr Meth Phys Res B45: 41–44

Ruck R, Dusausoy Y, Nguyen Trung C, Gaite J-M, Murciego A (1989) Powder EPR study of natural cassiterites and synthetic SnO_2 doped with Fe, Ti, Na and Nb. Eur J Mineral 1: 343–352

Sidorenko GA, Korovushkin VV, Gorshkov AI, Rudnizkaya ES, Dikov JP, Kauchova LV, Sivzov AV (1993) On the mineral nature of varlamoffite (in Russian). Mineral Shurnal 15: 94–101

Taylor RG, Morgan WR, Phillips DN (1970) On the occurrence of varlamoffite at the Sardine tin mine, North Queensland, Australia. Mineral Mag 37: 624–628

Vlassopoulos D, Rossman GR, Haggerty SE (1993) Coupled substitution of H and minor elements in rutile and the implications of high OH contents in Nb- and Cr-rich rutile from the upper mantle. Am Mineral 78: 1181–1191

Authors' addresses: *Z. Losos*, Institute of Geological Sciences, Masaryk University Brno, Kotlářská 2, 611 37 Brno, Czech Republic, e-mail: losos@sci.muni.cz; *A. Beran*, Institut für Mineralogie und Kristallographie, Universität Wien-Geozentrum, Althanstraße 14, A-1090 Wien, Austria, e-mail: anton.beran@univie.ac.at